Simulation of anyons with tensor network algorithms

R. N. C. Pfeifer,[1,*] P. Corboz,[1] O. Buerschaper,[2] M. Aguado,[2] M. Troyer,[3] and G. Vidal[1]
[1]*School of Mathematics and Physics, The University of Queensland, St Lucia, Queensland 4072, Australia*
[2]*Max-Planck-Institut für Quantenoptik, Hans-Kopfermann-Straße 1, D-85748 Garching, Germany*
[3]*Theoretische Physik, ETH Zurich, 8093 Zurich, Switzerland*
(Received 20 July 2010; published 29 September 2010)

Interacting systems of anyons pose a unique challenge to condensed-matter simulations due to their nontrivial exchange statistics. These systems are of great interest as they have the potential for robust universal quantum computation but numerical tools for studying them are as yet limited. We show how existing tensor network algorithms may be adapted for use with systems of anyons and demonstrate this process for the one-dimensional multiscale entanglement renormalization ansatz (MERA). We apply the MERA to infinite chains of interacting Fibonacci anyons, computing their scaling dimensions and local scaling operators. The scaling dimensions obtained are seen to be in agreement with conformal field theory. The techniques developed are applicable to any tensor network algorithm, and the ability to adapt these ansätze for use on anyonic systems opens the door for numerical simulation of large systems of free and interacting anyons in one and two dimensions.

DOI: 10.1103/PhysRevB.82.115126 PACS number(s): 05.30.Pr, 73.43.Lp, 02.70.−c

I. INTRODUCTION

The study of anyons offers one of the most exciting challenges in contemporary physics. Anyons are exotic quasiparticles with nontrivial exchange statistics, which makes them difficult to simulate. However, they are of great interest as some species offer the prospect of a highly fault-tolerant form of universal quantum computation,[1,2] and it has been suggested[3] that the simplest such species may appear in the fractional quantum Hall state with filling fraction $\nu=12/5$. Despite the current strong interest in the development of practical quantum computing, our ability to study the collective behavior of systems of anyons remains limited.

The study of interacting systems of anyons using numerical techniques was pioneered by Feiguin *et al.*,[4] using exact diagonalization for one-dimensional (1D) systems of up to 37 anyons, and the density-matrix renormalization-group (DMRG) algorithm[5] for longer chains. Also related is work by Sierra and Nishino,[6] later extended by Tatsuaki,[7] which applies a variant of DMRG to spin chain models having $SU(2)_k$ symmetry. Some of these models are now known to correspond to $SU(2)_k$ anyon chains,[8] and using this mapping these systems may also be studied using the Bethe ansatz[9] and quantum Monte Carlo.[10]

However, all of these methods have their limitations. Exact diagonalization has a computational cost which is exponential in the number of sites, strongly limiting the size of the systems which may be studied. DMRG is capable of studying larger system sizes but is typically limited to 1D or quasi-1D systems (e.g., ladders). Mapping to a spin chain is useful in one dimension but is substantially less practical in two. There are therefore good reasons to desire a formalism which will allow the application of other tensor network algorithms to systems of anyons. Many of these tensor networks, such as projected entangled pair states (PEPSs),[11–15] and the two-dimensional (2D) versions of Tree Tensor Networks (TTN) (Ref. 16) and of the multiscale entanglement renormalization ansatz (MERA) (Refs. 17–19) have been designed specifically to accurately describe two-dimensional systems.

In one dimension, many previously studied systems of interacting anyons display extended critical phases,[4,8] which are characterized by correlators exhibiting polynomial decay.[20] Whereas DMRG favors accurate representation of short-range correlators at the expense of long-range accuracy, the 1D MERA (Refs. 21 and 22) is ideally suited to this situation as its hierarchical structure naturally encodes the renormalization group flow at the level of operators and wave functions,[21–24] and hence accurately reproduces correlators across a wide range of length scales.[21,22,25–27] The development of a general formalism for anyonic tensor networks is therefore also advantageous for the study of 1D anyonic systems.

This paper describes how any tensor network algorithm may be adapted to systems of anyons in one or two dimensions using structures which explicitly implement the quantum group symmetry of the anyon model. As a specific example we demonstrate the construction of the anyonic 1D MERA, which we then apply to an infinite chain of interacting Fibonacci anyons at criticality. The approach which we present is completely general, and can be applied to any species of anyons and any tensor network ansatz.

II. ANYONIC STATES

Consider a lattice $\mathcal{L}_0$ of n sites populated by anyons. In contrast to bosonic and fermionic systems, for many anyon models the total Hilbert space $\mathbb{V}_{\mathcal{L}_0}$ cannot be divided into a tensor product of local Hilbert spaces. Instead, a basis is defined by introducing a specific fusion tree [e.g., Fig. 1, (i)]. The fusion tree is always constructed on a linear ordering of anyons, and while the 1D lattice naturally exhibits such an ordering, for 2D lattices some linear ordering must be imposed. Each line is then labeled with a charge index a_i such that the labels are consistent with the fusion rules of the anyon model,

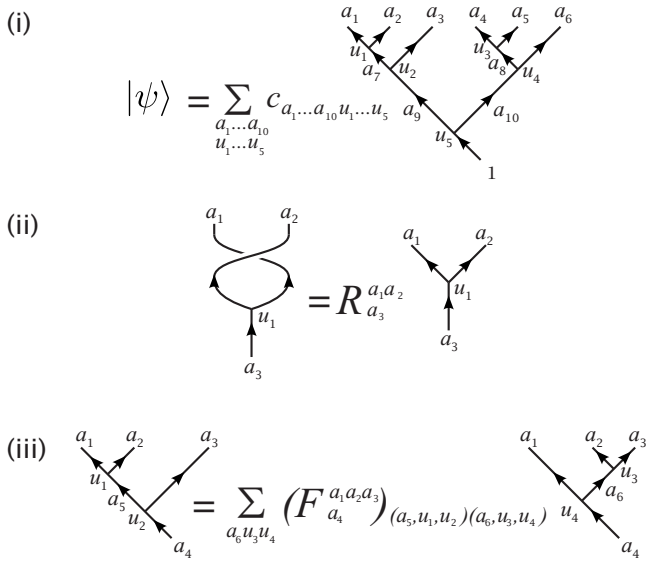

FIG. 1. (i) Example representation of a state $|\psi\rangle$ in a fusion tree basis for a system of six anyons. Labels a_i indicate charges associated with edges of the fusion tree graph, and labels u_i are degeneracies associated with vertices. The structure of the tree corresponds to a choice of basis and does not affect the physical content of the theory. (ii) Braiding may be used to change the ordering of the leaves of a fusion tree basis or to represent anyon exchange. (iii) F moves convert between the bases associated with different fusion trees.

$$a \times b \to \sum_c N_{ab}^c c. \tag{1}$$

For anyon types where some entries of the multiplicity tensor N_{ab}^c take values greater than 1, a label u_i is also affixed to the vertex which represents the fusion process to distinguish between the different copies of charge c. The edges of the graph which are connected to a vertex only at their lower end are termed "leaves" of the fusion tree, and we will associate these leaves with the charge labels $a_1, \ldots, a_n$. Different orderings of the leaves on a fusion tree may be interconverted by means of braiding [Fig. 1, (ii)], and different fusion trees, corresponding to different bases of states, may be interconverted by means of F moves [Fig. 1, (iii)].[28,29] In some situations it may also be useful to associate a further index b_i with each of the leaves of the fusion tree. For example, if the leaves are equated with the sites of a physical lattice, then this additional index may be used to enumerate additional nonanyonic degrees of freedom associated with that lattice. For simplicity we will usually leave these extra indices $b_1, \ldots, b_n$ implicit, as we have done in Fig. 1, as they do not directly participate in anyonic manipulations such as F moves and braiding.

Let the total number of charge labels on the fusion tree be given by m, where $m \geq n$. For Abelian anyons the fusion rules uniquely constrain all a_i for $i > n$, and provided there are no constraints on the total charge, the total Hilbert space reduces to a product of local Hilbert spaces $\mathbb{V}$, such that $\mathbb{V}_{\mathcal{L}_0} = \mathbb{V}^{\otimes n}$. For non-Abelian anyons, additional degrees of freedom arise because some fusion rules admit multiple outcomes, permitting certain a_i $(i > n)$ to take on multiple values while remaining consistent with the fusion rules, and the resulting Hilbert space does not necessarily admit a tensor product structure.

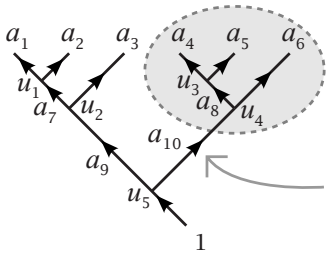

FIG. 2. The leaves of this fusion tree carry the charge labels a_1 to a_6. An edge which is not a leaf, labeled with charge a_{10}, is indicated by the large gray arrow. The portion of the fusion tree extending from edge a_{10} out to the leaves is indicated by the gray ellipse. If a degeneracy index μ_{10} is associated with charge a_{10}, then for a given value of a_{10}, index μ_{10} will enumerate all compatible labelings of the highlighted portion of the fusion tree.

We will now associate a parameter ν_{i,a_i} with each charge on the fusion tree, which we will term the degeneracy. This parameter corresponds to the number of possible fusion processes by which charge a_i may be obtained at location i. Where charge a_k arises from the fusion of charges a_i and a_j, then ν_{k,a_k} will satisfy

$$\nu_{k,a_k} = \sum_{a_i,a_j} \nu_{i,a_i} \nu_{j,a_j} N_{a_i a_j}^{a_k}. \tag{2}$$

For systems where the only degrees of freedom are anyonic, degeneracies on the physical lattice $\mathcal{L}_0$ (i.e., ν_{i,a_i}, $1 \leq i \leq n$) will take values of 0 or 1 depending on whether a charge a_i is permitted on lattice site i. Higher values of ν_{i,a_i} may be used on the physical lattice if there is also a need to represent additional nonanyonic degrees of freedom, enumerated by indices $b_1, \ldots, b_n$.

Up to this point we have parametrized our Hilbert space in terms of explicit labelings of the fusion tree. We now adopt a different approach: consider an edge i of the fusion tree which is not a leaf. As well as labeling this edge with a charge a_i we may introduce a second index μ_i, running from 1 to ν_{i,a_i}. Each pair of values $\{a_i, \mu_i\}$ may be associated with a unique charge labeling for the portion of the fusion tree from edge i out to the leaves, with these labelings being compatible with the fusion rules in the presence of a charge of a_i on site i (for an illustration of this, see Fig. 2). Provided we know the structure of the fusion tree above i and have a systematic means of associating labelings of that portion of the tree with values of μ_i, then in lieu of stating the values of all a_j for edges j involved in that portion of the tree, we may simply specify the value of the degeneracy index μ_i. In this way we may specify an entire state in the form

$$|\psi\rangle = \sum_{\mu_m} c_{a_m \mu_m} |a_m, \mu_m\rangle, \tag{3}$$

where a_m is the total charge obtained on fusing all the anyons. The index μ_m, which is the degeneracy index asso-

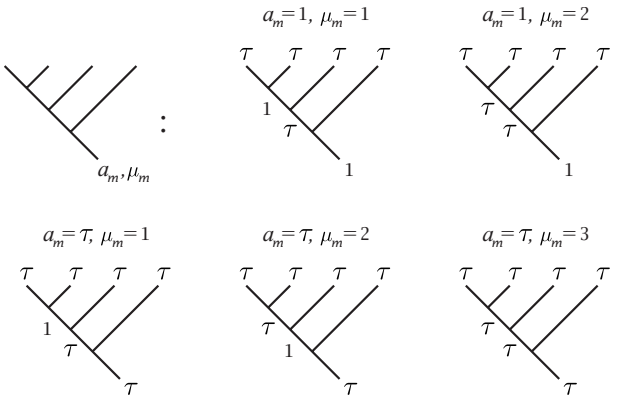

FIG. 3. Example enumeration of states according to a_m and μ_m for a fusion tree describing four Fibonacci anyons. The Fibonacci anyon model has one nonvacuum charge label (τ) and one nontrivial fusion rule, $\tau\times\tau\rightarrow 1+\tau$. Because the charges 1 and τ are both self-dual, no arrows are required on diagrammatic representations of Fibonacci anyon fusion trees.

ciated with the total charge of the fusion tree, may be understood as systematically enumerating all possible labelings of the entire fusion tree including charge labels, vertex labels, and any labels associated with additional nonanyonic degrees of freedom. For example, see Fig. 3. Note that for a given edge i, the value of the degeneracy ν_{i,a_i} may vary with the charge a_i and consequently the range of the degeneracy index μ_m in Eq. (3) is dependent on the value of the charge a_m.

The notation of Eq. (3) should be contrasted with that of Fig. 1, (i). In the latter, the number of indices on c depends on the number of charge labels on the fusion tree, whereas in the former, the tensor describing the state is always indexed by just one pair of labels—charge and degeneracy—which will prove advantageous in constructing a tensor network formalism for systems of anyons.

We now choose to restrict our attention to systems having the identity charge. We may do this without loss of generality as a state on n lattice sites with a total charge a_m may always be equivalently represented by a state on $n+1$ lattice sites whose total charge is the identity, with a charge $\overline{a_m}$ on lattice site $n+1$. This additional charge annihilates the total charge a_m of sites $1,\ldots,n$ to give the vacuum. The expression for $|\psi\rangle$ then becomes

$$|\psi\rangle = \sum_{\mu_{m'}} c_{1\mu_{m'}}|1,\mu_{m'}\rangle, \tag{4}$$

where $\mu_{m'}$ ranges from 1 to the dimension of the Hilbert space of the system of n sites with total charge a_m. Consequently we may represent the state $|\psi\rangle$ of a system of anyons by means of the vector $c_{1\mu_{m'}}$. For simplicity of notation, we will take Greek indices from the beginning of the alphabet to correspond to pairs of indices $\{a_i,\mu_i\}$ consisting of a charge index and the associated degeneracy index. The vector $c_{1\mu_{m'}}$ will therefore be denoted simply c^α, with the understanding that in this case the charge component $a_{m'}$ of multi-index α takes only the value 1. (Multi-index α is raised as we will shortly introduce a diagrammatic formalism in which vector c is represented by an object with a single upward-going leg. In this formalism, upward- and downward-going legs may be associated with upper and lower multi-indices, respectively.)

III. ANYONIC OPERATORS

We will divide our consideration of anyonic operators into two parts. First we shall consider operators which map a state on some Hilbert space $\mathcal{H}$ into another state on the same Hilbert space. When applied to a state represented by c^α, such an operator leaves the degeneracies of the charges in multi-index α unchanged. We will therefore call these *degeneracy-preserving* anyonic operators. Then we will consider those operators which map a state on some Hilbert space $\mathcal{H}$ into a state on some other Hilbert space $\mathcal{H}'$. These operators may represent processes which modify the environment, for example, by adding or removing lattice sites, and also play an important part in anyonic tensor networks, for instance taking the role of isometries in the TTN and MERA. As these operators can change the degeneracies of charges in a multi-index α, we will call them *degeneracy-changing* anyonic operators. More generally, the degeneracy-preserving anyonic operators may be considered a subclass of the degeneracy-changing anyonic operators for which $\mathcal{H}=\mathcal{H}'$.

A. Degeneracy preserving anyonic operators

We begin with those operators which map states on some Hilbert space $\mathcal{H}$ into other states on the same Hilbert space $\mathcal{H}$. Examples of these operators include Hamiltonians, reduced density matrices, and unitary transformations such as the disentanglers of the MERA.

First, we introduce splitting trees. The space of splitting trees is dual to the space of fusion trees. While the space of fusion trees consists of labeled directed graphs whose number of branches increases monotonically when read from bottom to top, the space of splitting trees consists of labeled directed graphs whose number of branches increases monotonically when read from top to bottom. An inner product is defined by connecting the leaves of fusion and splitting trees which have equivalent linear orderings of the leaves (braiding first if necessary), then eliminating all loops as per Fig. 4, (i), with F moves performed as required.

Anyonic operators may always be written as a sum over fusion and splitting trees, such as the two-site operator $\hat{M}$ shown in Fig. 4, (ii), and for degeneracy-preserving anyonic operators it is always possible to choose the splitting tree to be the adjoint of the fusion tree. To apply an operator to a state the two corresponding diagrammatic representations are connected as shown in Fig. 4, (iii), and closed loops may be eliminated as shown in Fig. 4, (i). Sequences of F moves, braiding, and loop eliminations may be performed until the diagram has been reduced once more to a fusion tree without loops on a lattice of n sites.

Much as the state of an anyonic system may be represented by a vector c^α, anyonic operators may be represented by a matrix M^β_α. Each value of α corresponds to a pair $\{a_i,\mu_i\}$, where a_i is a possible charge of the central edge of

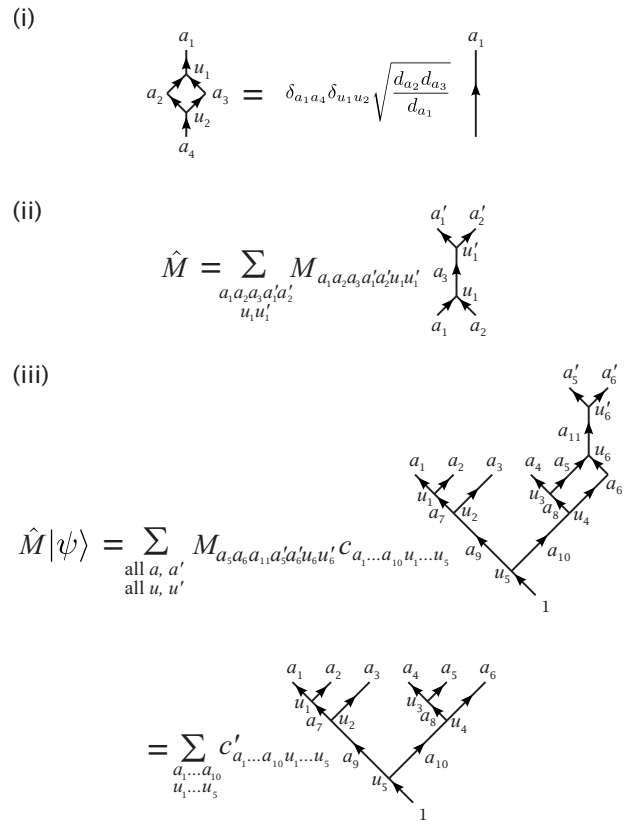

FIG. 4. (i) Loops are eliminated by replacing them with an equivalent numerical factor determined by the normalization convention. The factor given here corresponds to the diagrammatic isotopy convention employed in Ref. 29. (ii) Definition of a simple two-site anyonic operator. (iii) Application of an operator to a state is performed by connecting the diagrams' free legs. By performing F moves and eliminating loops (and in more complex examples, also braiding) it is possible to obtain an expression for the resulting state in the original basis.

the operator diagram [e.g., a_3 in Fig. 4, (ii)], and μ_i is a value of the degeneracy index associated with charge a_i. We will denote the degeneracy of a_i by ν_{a_i}. Similarly, values of β correspond to pairs $\{a_j, \mu_j\}$, where a_j has degeneracy ν_{a_j}. For degeneracy-preserving anyonic operators the charge indices a_i and a_j necessarily take on the same range of values, and $\nu_{a_i} = \nu_{a_j}$ when $a_i = a_j$. The values of ν_{a_i} may equivalently be calculated from either the fusion tree making up the top half or the splitting tree making up the bottom half of the operator diagram.

A well-defined anyonic operator $\hat{M}$ must respect the (quantum) symmetry group of the anyon model, and consequently all entries in M_α^β for which $a_i \neq a_j$ will be zero. However, in contrast with c^α we do not require that $a_i = a_j = 1$. When $\hat{M}$ is a degeneracy-preserving operator, matrix M_α^β is therefore a square matrix of side length

$$\ell_M = \sum_{a_i} \nu_{a_i}, \tag{5}$$

which may be organized to exhibit a structure which is block diagonal in the charge indices a_i and a_j, and for which the blocks are also square. As an example consider Fig. 5, which shows an operator acting on four Fibonacci anyons. An example matrix M_α^β for an operator of this form is given in Table I, from which the entries of M_{abcde} can be reconstructed, e.g., $M_{\tau 1 \tau 1 \tau} = 3$.

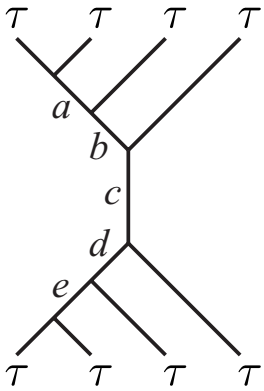

FIG. 5. An operator acting on four Fibonacci anyons. The values of the coefficients M_{abcde} may be specified as a block-diagonal matrix M_α^β, for example, as in Table I.

TABLE I. Matrix representation M_α^β for an example operator of the form shown in Fig. 5. Multi-index α corresponds to index pair $\{a_i, \mu_i\}$ and multi-index β corresponds to pair $\{a_j, \mu_j\}$. Subject to an appropriate ordering convention for μ_i and μ_j, these indices may be related to the fusion tree labels a, b, c, d, and e of Fig. 5 as shown. Note that as c is the charge on the central leg of Fig. 5, all nonzero entries of M_α^β satisfy $a_i = a_j = c$.

$M_\alpha^\beta =$

a_i, μ_i \ a_j, μ_j	1,1	1,2	τ,1	τ,2	τ,3
1,1	1	0.5	0	0	0
1,2	0.5	1	0	0	0
τ,1	0	0	1	2	−1
τ,2	0	0	2	3	−1
τ,3	0	0	1	1	1

a_i	μ_i	a	b	c
1	1	1	τ	1
1	2	τ	τ	1
τ	1	1	τ	τ
τ	2	τ	1	τ
τ	3	τ	τ	τ

a_j	μ_j	e	d	c
1	1	1	τ	1
1	2	τ	τ	1
τ	1	1	τ	τ
τ	2	τ	1	τ
τ	3	τ	τ	τ

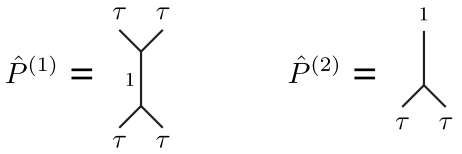

FIG. 6. Diagrammatic representation of operators $\hat{P}^{(1)}$ (6) and $\hat{P}^{(2)}$ (7). The charges on all leaves are nondegenerate.

B. Degeneracy-changing anyonic operators

We now introduce the second class of anyonic operators, which map states in some Hilbert space $\mathcal{H}$ into some other Hilbert space $\mathcal{H}'$. These operators may reduce or increase the degeneracy of any charge present in the spaces on which they act, and may even project out entire charge sectors by setting their degeneracy to zero. When these operators are written in the conventional notation of Fig. 4, the fusion and splitting trees will not be identical. Further, we may choose to allow combinations of degeneracies which do not naturally admit complete decomposition into individual anyons. For example, a degeneracy-changing operator may map a state on five Fibonacci anyons (having total degeneracies $\nu_1=3$ and $\nu_\tau=5$) into a state having degeneracies $\nu_1=2$ and $\nu_\tau=2$. As these degeneracies do not admit decomposition into an integer number of nondegenerate anyons, it is necessary to associate an index u_i with the single open leg of the fusion tree. This index behaves identically to the vertex indices u_i of Fig. 1, serving to enumerate the different copies of each individual charge, and as with the vertex indices of Fig. 1, it is absorbed into the degeneracy index μ_i.

As a further example, a state having degeneracies $\nu_1=4$ and $\nu_\tau=4$ could be associated with a fusion tree having either one leg or two legs each with degeneracies $\nu_1=0$ and $\nu_\tau=2$. Again, indices u_i would have to be associated with each open leg.

Matrix representations of degeneracy-changing anyonic operators may also be constructed, and when they are written in block-diagonal form, the matrices and their blocks may be rectangular rather than square. Degeneracy-changing anyonic operators therefore represent a generalization of the degeneracy-preserving anyonic operators discussed in Sec. III A. It is worth noting that the presence of indices u_i on the open legs of the fusion or splitting trees of an operator do not automatically imply that it is a degeneracy-changing anyonic operator: The defining characteristic of a degeneracy-preserving anyonic operator is that it maps a state in a Hilbert space $\mathcal{H}$ into a state in the same Hilbert space $\mathcal{H}$, and consequently both the matrix as a whole and all of its blocks are square. Thus a degeneracy-preserving anyonic operator may act on states having additional indices u_i on their open legs, and the resulting state may be expressed in the form of the same fusion tree, with the same additional indices on the open legs.

Operators which change degeneracies may represent physical processes which change the accessible Hilbert space of a system. As we will see in Sec. V A, they may also be used in tensor network algorithms as part of an efficient representation of particular states or subspaces of a Hilbert space, for example the ground state or the low-energy sector of a local Hamiltonian.

This distinction between degeneracy-changing and degeneracy-preserving anyonic operators is clearly seen with a simple example. Let $|\psi\rangle$ be a state on six Fibonacci anyons. This state can be parametrized by a vector c^α, which has five components. We now define two projection operators, $\hat{P}^{(1)}$ and $\hat{P}^{(2)}$ (Fig. 6), each of which acts on the fusion space of anyons τ_1 and τ_2. Operator $\hat{P}^{(1)}$ is degeneracy preserving, and projects c^α into the subspace in which anyons τ_1 and τ_2 fuse to the identity. Its matrix representation is

$$P_\alpha^{(1)\beta}=\begin{pmatrix}1 & 0\\ 0 & 0\end{pmatrix}, \tag{6}$$

where the first value of each multi-index corresponds to a charge of 1 and the second to a charge of τ. Operator $\hat{P}^{(2)}$ performs the same projection but is degeneracy changing. Its matrix representation is written

$$P_\alpha^{(2)\beta}=(1 \quad 0). \tag{7}$$

Both operators perform equivalent projections, in the sense that

$$\langle\psi|\hat{P}^{(1)\dagger}\hat{P}^{(1)}|\psi\rangle=\langle\psi|\hat{P}^{(2)\dagger}\hat{P}^{(2)}|\psi\rangle. \tag{8}$$

When $\hat{P}^{(1)}$ acts on $|\psi\rangle$ it leaves the Hilbert space unchanged, and hence the vector c'^α describing state $|\psi'\rangle=\hat{P}^{(1)}|\psi\rangle$ is once again a five-component vector, although in an appropriate basis some components will now necessarily be zero. In contrast $\hat{P}^{(2)}$ explicitly reduces the dimension of the Hilbert space, and the vector c''^α describing state $|\psi''\rangle=\hat{P}^{(2)}|\psi\rangle$ is of length two, describing a fusion tree on only four Fibonacci anyons (as both τ_1 and τ_2 have been eliminated). One consequence of this distinction is that while $(\hat{P}^{(1)})^2=\hat{P}^{(1)}$, the value of $(\hat{P}^{(2)})^2$ is undefined.

IV. ANYONIC TENSOR NETWORKS

A. Diagrammatic notation

The diagrammatic notation conventionally employed in the study of anyonic systems, and used here in Figs. 1 and 4, is well suited to the complete description of anyonic systems, as it provides a physically meaningful depiction of the entire Hilbert space. However, the number of parameters required for such a description grows exponentially in the system size, and because it is necessary to explicitly assign every index to a specific charge or degeneracy, specification of a tensor network rapidly becomes inconveniently verbose [for example, see Fig. 4, (iii)].

In the preceding sections, we developed techniques whereby anyonic states and operators could be represented as vectors and matrices, bearing only one or two multi-indices apiece. We now introduce the graphical notation which complements this description, and in which we will formulate anyonic tensor networks. Fig. 7(i) gives the graphical representations of a state $|\psi\rangle$ associated with a vector c^α, and of an operator $\hat{M}$ associated with a matrix M_α^β. The circle marked c corresponds to the vector c^α, and the circle marked

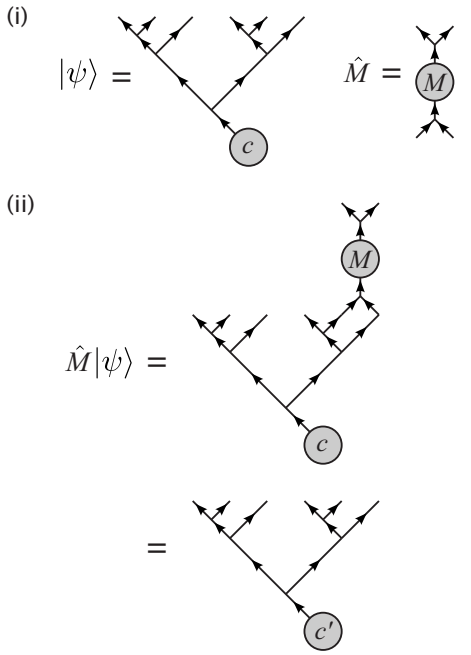

FIG. 7. (i) Diagrammatic representation of a state $|\psi\rangle$ and two-site operator $\hat{M}$ expressed in terms of degeneracy indices. (ii) Application of $\hat{M}$ to state $|\psi\rangle$. Gray shapes represent tensors with charge and degeneracy multi-indices, with each leg of the shape corresponding to one charge and degeneracy index pair. These diagrams represent the same state, operator, and process as Fig. 1, (i) and Fig. 4, (ii) and (iii).

M corresponds to the matrix M^{β}_{α}. In general, gray circles correspond to tensors, and the number of legs on the circle corresponds to the number of multi-indices on the associated tensor. Each multi-index is also associated with a fusion or splitting tree structure, which is specified graphically. For reasons to be discussed shortly, we will require that no tensor ever have more than three multi-indices. As the legs of the gray shapes are each associated with a multi-index, they carry both degeneracy and charge indices. Consequently it is not necessary to explicitly assign labels to the fusion/splitting trees, as these labelings are contained implicitly in the degeneracy index (for example, see Table I, where specifying the values of $\{a_i,\mu_i\}$ and $\{a_j,\mu_j\}$ is equivalent to fully labeling the fusion and splitting trees of Fig. 5).

The fusion or splitting tree associated with a particular multi-index may be manipulated in the usual way by means of braids and F moves, recalling that each component of the tensor is associated with a particular labeling of the fusion and splitting trees via the corresponding values of the multi-indices. Manipulations performed upon a particular tree thus generate unitary matrices which act upon the multi-index that corresponds to the labelings of that particular tree.

The application of an operator to a state is, unsurprisingly, performed by connecting the appropriate diagrams, as shown in Fig. 7, (ii). For operators of the type discussed in Sec. III A, the outcome is necessarily a new state in the same Hilbert space, which consequently can be described by a new state vector c'^{α}, as shown. However, in general an operator $\hat{M}$ will not act on the entire Hilbert space of the system, and so will be described by a tensor constructed on the fusion space of some subset of lattice sites, and not on the system as a whole. Operator $\hat{M}$ acting on state $|\psi\rangle$ in Fig. 7, (ii) is an example of this. Because c^{α} describes a six-site system but M^{β}_{α} is constructed on the fusion space of two sites, the multi-indices of M^{β}_{α} span a significantly smaller Hilbert space than that of c^{α} and we cannot simply write

$$c'^{\beta} = c^{\alpha} M^{\beta}_{\alpha} \tag{9}$$

(using Einstein notation, where repeated multi-indices are assumed to be summed). Instead, we must understand how to expand the matrix representation of an operator on some number of sites x, to obtain its matrix representation as an operator on x' sites, where $x' > x$.

B. Site expansion of anyonic operators

The multiplicity tensor N^{c}_{ab} describes the fusion of two charges without degeneracies. It is easily extended to incorporate degeneracies of the charges, and we will denote this expanded multiplicity tensor $\tilde{N}^{\gamma}_{\alpha\beta u}$ where multi-indices α, β, and γ are associated with the pairs $\{a,\mu_a\}$, $\{b,\mu_b\}$, and $\{c,\mu_c\}$, respectively, and for given values of α, β, and γ, u runs from 1 to N^{c}_{ab}. The degeneracies associated with charges a, b, and c are denoted ν_a, ν_b, and ν_c, respectively. As with μ_a, μ_b, and μ_c, there is an implicit additional index on each degeneracy ν_x representing the edge of the tree on which charge x resides. The values of ν_a and ν_b may be chosen arbitrarily (for example, $\nu_a|_{a=1}$ may differ from $\nu_b|_{b=1}$) but the degeneracies associated with the values of c must satisfy

$$\nu_c = \sum_{a,b} \nu_a \nu_b N^{c}_{ab} \tag{10}$$

in accordance with Eq. (2). When this constraint is satisfied, every quadruplet of indices $\{a,\mu_a,b,\mu_b\}$ corresponding to a unique pair of choices for α and β may be associated with N^{c}_{ab} distinct pairs of indices $\{c,\mu_c\}$ for each $c \in a \times b$. These pairs $\{c,\mu_c\}$ are enumerated by the additional index u. This defines a 1:1 mapping between sets of values on $\{a,\mu_a,b,\mu_b,u\}$ and pairs $\{c,\mu_c\}$, and we set the corresponding entries in $\tilde{N}^{\gamma}_{\alpha\beta u}$ to 1, with all other entries being zero. A simple example is given in Table II.

By virtue of their derivation from N^{c}_{ab}, the object $\tilde{N}^{\gamma}_{\alpha\beta u}$ and its conjugate $\tilde{N}^{\dagger\alpha\beta u}_{\gamma}$ represent application of the anyonic fusion rules, and may be associated with vertices of the splitting and fusion trees. Under the isotopy invariance convention there is an additional factor of $[d_c/(d_a d_b)]^{1/4}$ associated with the fusion of charges a and b into c, where d_x is the quantum dimension of charge x, and similarly for splitting, but we will account for these factors separately. Thus constructed, the tensors $\tilde{N}$ satisfy $\tilde{N}^{\gamma}_{\alpha\beta u}\tilde{N}^{\dagger\alpha\beta u}_{\epsilon} = \delta^{\gamma}_{\epsilon}$.

When used as a representation of the fusion rules, the generalized multiplicity tensor $\tilde{N}^{\gamma}_{\alpha\beta u}$ and its conjugate $\tilde{N}^{\dagger\alpha\beta u}_{\gamma}$ permit us to increase or decrease the number of multi-indices on a tensor in a manner which is consistent with the fusion rules of the quantum symmetry group. This process is reversible provided the symmetry group is Abelian or, for a non-

TABLE II. Construction of $\tilde{N}^{\gamma}_{\alpha\beta u}$ for a fusion vertex for Fibonacci anyons. In this example a may take charges 1 and τ each with degeneracy 1, and b may take charges 1 and τ with degeneracies 1 and 2, respectively. By Eq. (2), charge c may therefore take values 1 and τ with degeneracies 3 and 5, respectively. A correspondence between the values of multi-index γ and of multi-indices α and β is established in some systematic manner, with each assignation satisfying $c \in a \times b$, and for Fibonacci anyons the index u is trivial as all multiplicities N^{c}_{ab} are zero or one. An example assignation is shown in the table. The corresponding entries of $\tilde{N}$ are then set to 1, with all other entries zero. For example, the fourth row indicates that $\tilde{N}^{(\tau,1)}_{(1,1)(\tau,1)1}=1$.

Pair $\{c,\mu_c\}$	Assigned pentuplet $\{a,\mu_a,b,\mu_b,u\}$
1, 1	1, 1, 1, 1, 1
1, 2	τ, 1, τ, 1, 1
1, 3	τ, 1, τ, 2, 1
τ, 1	1, 1, τ, 1, 1
τ, 2	1, 1, τ, 2, 1
τ, 3	τ, 1, 1, 1, 1
τ, 4	τ, 1, τ, 1, 1
τ, 5	τ, 1, τ, 2, 1

Abelian symmetry group, provided the total number of multi-indices on the tensor does not at any time exceed three. In constructing and manipulating a tensor network for a system of anyons, we will require only objects which respect the fusion rules of the anyon model. It is a defining property of such objects that when the number of multi-indices they possess is reduced to 1 by repeated application of $\tilde{N}$ and $\tilde{N}^{\dagger}$, nonzero entries may be found only in the vacuum sector. We imposed this requirement for states in Sec. II, and it is equivalent to the restriction we imposed on anyonic operators in Sec. III A. In Ref. 30 an equivalent condition was observed for tensors remaining unchanged under the action of a Lie group, and these tensors were termed *invariant*. When working with invariant tensors, we may separately evaluate the components of the tensors acting on the degeneracy spaces (e.g., the nonzero blocks of M^{β}_{α}), and the factors arising from loops and vertices of the associated spin network. This property greatly simplifies the contraction of pairs of tensors.

In addition to increasing or decreasing the number of legs of a tensor, we may also use $\tilde{N}$ to "raise" the matrix representation of an operator from the space of x sites to the space of $(x+x')$ sites. This is shown in Fig. 8, and the matrix representation of the raised operator is given by

$$M'^{\beta}_{\alpha} = M^{\delta}_{\gamma}\tilde{N}^{\dagger\gamma\epsilon u}_{\alpha}\tilde{N}^{\beta}_{\delta\epsilon u}, \tag{11}$$

where multi-index ϵ describes the fusion space of all sites in $(x+x')$ but not in x. Because the numeric factors associated with loops, vertices, and braiding (where applicable) are handled separately, no factors of quantum dimensions appear in Eq. (11).

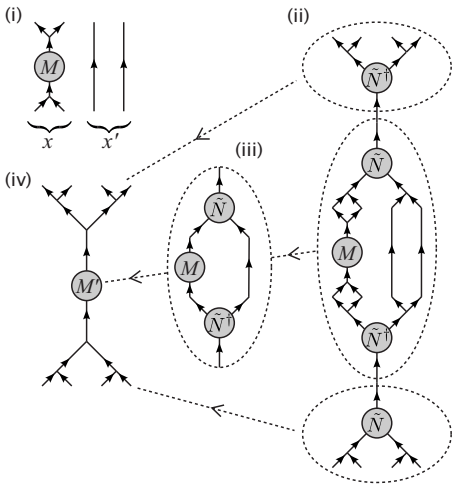

FIG. 8. "Raising" of an operator $\hat{M}$ from sites x to sites $x+x'$: (i) operator $\hat{M}$ defined only on sites denoted x. (ii) Resolutions of the identity are inserted above and below $\hat{M}$, being constructed from tensors $\tilde{N}$ and $\tilde{N}^{\dagger}$. The central portion of this diagram is identified as corresponding to the new matrix M'^{β}_{α} which describes $\hat{M}$ on $x+x'$. (iii) Loop and vertex factors in the central region are evaluated separately and eliminated. (iv) The tensor network corresponding to the new central portion is contracted. The $\tilde{N}$ and $\tilde{N}^{\dagger}$ tensors outside the central region become vertices of the fusion and splitting trees associated with M'^{β}_{α}. Together the trees and the matrix M'^{β}_{α} constitute the raised version of $\hat{M}$.

To act an operator $\hat{M}$ on a state $|\psi\rangle$ in the matrix representation, we therefore connect the diagrams for $\hat{M}$ and $|\psi\rangle$, eliminate all loops, and then raise the matrix representation of the operator $\hat{M}$ using Eq. (11), repeatedly if necessary, until the resulting matrix M'^{β}_{α} may be applied directly to the state vector c^{α}. Similarly it is possible to combine the matrix representations of operators, by connecting their diagrams appropriately, eliminating loops, and performing any required raising so that both operators act on the same fusion space. Their matrix representations can then be combined to yield the matrix representation of the new operator,

$$M^{(1\times 2)\beta}_{\alpha} = M^{(1)\gamma}_{\alpha}M^{(2)\beta}_{\gamma} \tag{12}$$

and the fusion/splitting tree associated with this new operator is obtained as shown in Fig. 8.

Note that as yet, we have not described how two objects may be combined if their multi-indices are both up or both down, and are connected by a curved line. To contract such objects together, it is necessary to understand how bends act on the central matrix of an operator. Once this is understood, the bend can be absorbed into one of the central matrices so that the connection is once again between an upper multi-index and a lower multi-index as in Eq. (12). This process is described in Sec. IV C.

C. Manipulation of anyonic operators

As observed in Sec. IV B, when we describe a system entirely in terms of objects invariant under the action of the

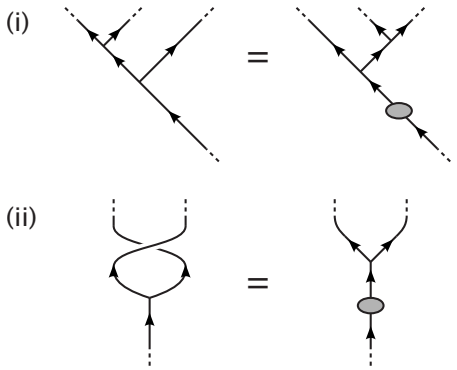

FIG. 9. (i) F move and (ii) braiding, performed on a section of fusion tree in the diagrammatic notation of Sec. IV A.

symmetry group, we may account separately for the numerical normalization factors associated with the spin network. However, as well as affecting these numerical factors, transformations of the fusion or splitting tree of an anyonic operator will typically also generate unitary matrices which act on the matrix representation of the operator. These matrices respect the symmetry of the anyon model, and thus can be written as block-diagonal matrices where each block is a unitary matrix acting on a particular charge sector. In terms of the diagrammatic notation of Sec. IV A, F moves and braids therefore result in the insertion of a unitary matrix, as shown in Fig. 9. These matrices, whose entries are derived from the tensors $(F_d^{abc})_{(eu\nu)(fu'v')}$ and R_c^{ab}, respectively, are raised if required, as described in Sec. IV B, and then contracted with M_α^β, the matrix representation of the operator. To compute the unitary matrices involved, it suffices to recognize that F moves and braids are unitary transformations in the space of labeled tree diagrams. Identifying the leg on which the unitary matrix is to be inserted, the relevant region of the space of labeled diagrams is then enumerated by the multi-index which can be associated with this leg (compare Fig. 2).

Braiding is of particular importance when working in two dimensions, as an operator will necessarily be defined with respect to some arbitrary linear ordering of its legs, and when manipulating a tensor network it may be necessary to map between this original definition and other equivalent definitions, corresponding to different leg orderings. For example, let $\hat{M}$ be a four-site anyonic operator as shown in Fig. 10, (i), which we wish to apply to a 2D lattice. For the indicated linearization of this lattice, application of $\hat{M}$ will require braiding as shown in Fig. 10, (ii). By evaluating the unitary transformations corresponding to these braids and absorbing them into M_α^β, we may define a new operator $\hat{M}'$ which acts directly on the linearized lattice without any intervening manipulations of the fusion/splitting trees.

We will also frequently wish to deal with tensor legs which bend vertically through 180°. If working with an anyon model that has nontrivial Frobenius-Schur indicators, then indicator flags must be applied to all bends. Like F moves and braiding, the reversal of a Frobenius-Schur indicator flag is a unitary transformation, and once again this leads to the introduction of a unitary matrix which can be

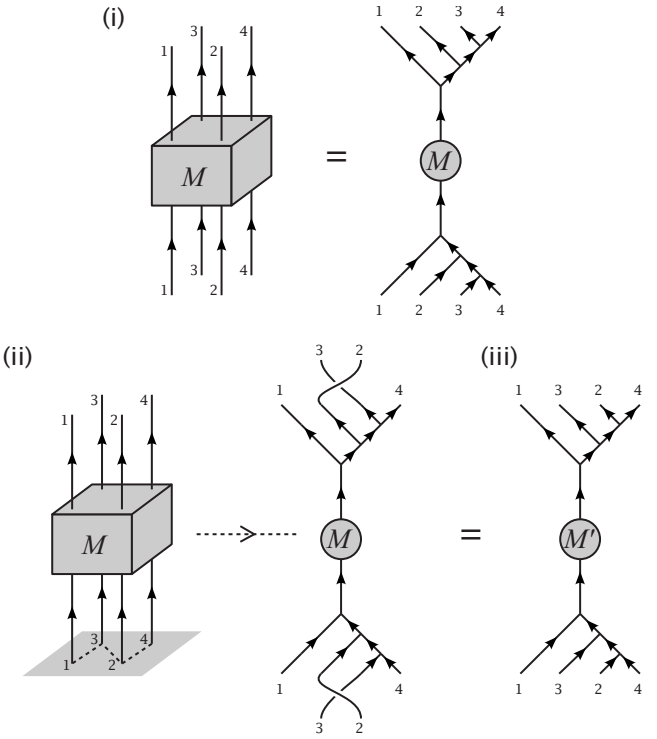

FIG. 10. (i) An operator $\hat{M}$ acting on sites on a 2D lattice is defined with respect to some arbitrary linear ordering of these sites. (ii) When manipulating the tensor network, it may on occasion be computationally convenient for the lattice to be linearized according to some alternative linearization scheme. In this example, the imposed linearization scheme is indicated by the dotted line. To apply $\hat{M}$ to a different linearization of the lattice may require braiding. The orientation of the braids can be determined by putting the fusion tree of (i) onto the 2D lattice, then smoothly deforming the lattice into a chain in accordance with the linearization prescription. (iii) The unitary matrices corresponding to the required F moves and braiding operations may be absorbed into $\hat{M}$, defining a new operator $\hat{M}'$ on the linearized lattice.

absorbed into a nearby existing tensor. However, we may wish to perform other operations on bends, such as absorbing them into fusion vertices or the central matrices of anyonic operators. We may also need to move a matrix M_α^β across a bend. We must therefore develop the description of bends in the new diagrammatic formalism.

In Ref. 29 a prescription for absorbing bends into fusion vertices is given in terms of tensors $(A_c^{ab})_{u\nu}$ and $(B_c^{ab})_{u\nu}$, derived from the F moves, and corresponding to clockwise and counter-clockwise bends, respectively. The absorption of a clockwise or counterclockwise bend into a fusion vertex is reproduced in Fig. 11, (i), and results in a vertex fusing upward- and downward-going legs. We now assign new tensors $(\tilde{N}^{\mathrm{CW}})^{\dagger\alpha u}_{\gamma\beta}$ and $(\tilde{N}^{\mathrm{CCW}})^{\dagger\beta u}_{\alpha\gamma}$ to such vertices, such that writing these transformations in the notation of Sec. IV A is trivial. This is shown in Fig. 11, (ii).

Explicit expressions for the new vertex tensors $(\tilde{N}^{\mathrm{CW}})^\dagger$ and $(\tilde{N}^{\mathrm{CCW}})^\dagger$ may be obtained by recognizing that Fig. 11, (i) describes the action of unitary transformations on $\tilde{N}^{\dagger\alpha\beta u}_\gamma$. When the bend is counterclockwise, the corresponding uni-

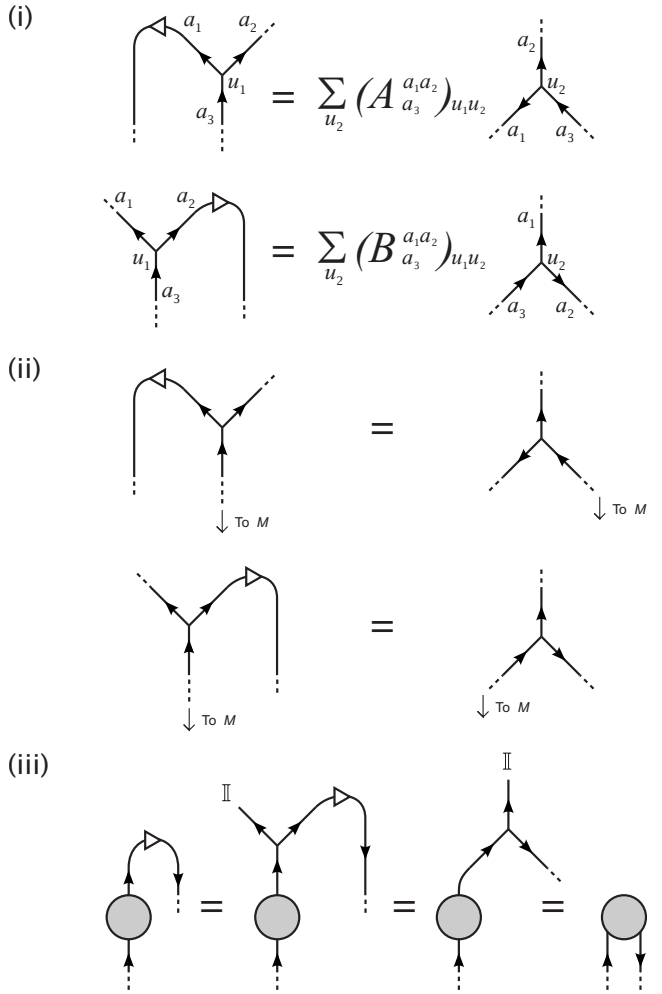

FIG. 11. Vertical bending of legs (i) in the standard diagrammatic notation and (ii) in the diagrammatic notation of Sec. IV A. White triangles represent Frobenius-Schur indicator flags. (iii) Legs on the matrix representations of states and operators may also absorb bends.

tary matrix is derived from $(A_c^{ab})_{uv}$, and when the bend is clockwise, the unitary matrix is derived from $(B_c^{ab})_{uv}$. We will denote these unitary matrices A_γ^δ and B_γ^δ, respectively. We then have

$$(\tilde{N}^{\mathrm{CW}})^{\dagger\alpha u}_{\gamma\beta} = A^\delta_\gamma \tilde{N}^{\dagger\alpha\epsilon u}_\delta \delta_{\epsilon\beta}, \tag{13}$$

$$(\tilde{N}^{\mathrm{CCW}})^{\dagger\beta u}_{\alpha\gamma} = B^\delta_\gamma \tilde{N}^{\dagger\epsilon\beta u}_\delta \delta_{\epsilon\alpha}. \tag{14}$$

and conjugation describes equivalent vertices $\tilde{N}^{\mathrm{CW}}$ and $\tilde{N}^{\mathrm{CCW}}$ when a bend is absorbed into a splitting tree.

Knowing how the absorption of bends acts on a vertex tensor, we may readily infer how the same process acts on the matrix representation of an operator. In Fig. 11, (iii) we see a bend absorbed into the matrix M^β_α, resulting in a new object with two lower multi-indices, $M'_{\alpha\beta}$. First we exploit the freedom to introduce fusion with the trivial charge (denoted $\mathbb{I}$), with degeneracy 1. The corresponding $\tilde{N}^\dagger$ object takes only one value on its upper left multi-index, and is

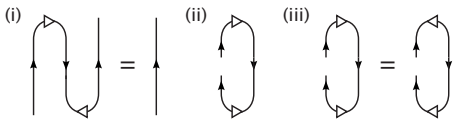

FIG. 12. Opposing pairs of Frobenius-Schur indicators (i) on a pair of bends equivalent to the identity and (ii) on a pair of bends such as might be used when computing a quantum trace. (iii) As an anyon model can always be specified such that the Frobenius-Schur indicators are ± 1, reversing a pair of contiguous opposed Frobenius-Schur indicator flags is always free.

fully defined by $\tilde{N}^{\dagger 1\beta 1}_\gamma = \delta^\beta_\gamma$. Absorbing the bend into this fusion vertex as per Eq. (13) yields $A^\delta_\gamma \delta^\epsilon_\delta \delta_{\epsilon\beta} = A_{\gamma\beta}$, which may be then combined with M^β_α to give

$$M'_{\alpha\beta} = M^\gamma_\alpha A_{\gamma\beta}. \tag{15}$$

In conjunction with the relationships given in Fig. 12, this gives us the ability to move a matrix past a bend. An example of this is given in Fig. 13, for which M and M' are related according to

$$M'^\beta_\alpha = A_{\alpha\gamma} M^\gamma_\delta \varkappa^\delta_\epsilon B^{\dagger\epsilon\beta}, \tag{16}$$

where $\varkappa^\delta_\epsilon$ represents reversal of the Frobenius-Schur indicator flag on the lower bend. Finally, bending may also allow more efficient contraction of pairs of anyonic operators, as shown in Fig. 14.

Having described the action of bends, it is customary also to introduce a second type of F move which is described by the tensor $(F^{a_1a_2}_{a_3a_4})_{(a_5u_1u_2)(a_6u_3u_4)}$ (Fig. 15). This tensor may be derived from $(F^{a_1a_2a_3}_{a_4})_{(a_5u_1u_2)(a_6u_3u_4)}$ by bending, and as with $(F^{a_1a_2a_3}_{a_4})_{(a_5u_1u_2)(a_6u_3u_4)}$ these F moves perform a transformation of the fusion tree, accompanied by the introduction of a unitary matrix which can be absorbed into the matrix representation of the operator. These unitary matrices correspond to the consecutive application of a bend, an F move of the original type, and a second bend whose action is the inverse of the first.

D. Constructing a tensor network

Now that we have developed a formalism for anyonic tensors, we may convert an existing tensor network algorithm for use with anyons. First, the tensor network must be drawn in such a manner that every leg has a discernible vertical orientation. Although these orientations may be changed during manipulation of the tensor network, an initial

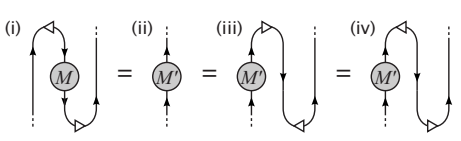

FIG. 13. Moving a matrix across a bend in a tensor network diagram. (i) Initial diagram. (ii) Bends are absorbed into the matrix. (iii) New bends are introduced, in accordance with Fig. 12, (i). (iv) A pair of contiguous, opposed Frobenius-Schur indicators are reversed, as per Fig. 12, (iii). The initial and final matrices M and M' are related as specified in Eq. (16).

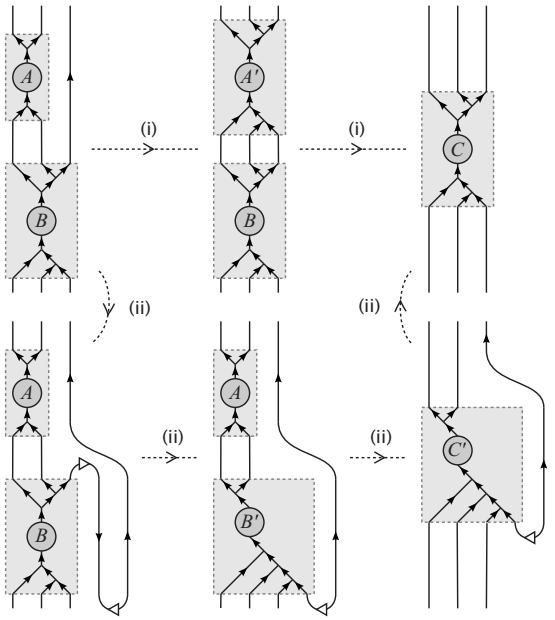

FIG. 14. The use of bends may permit the more efficient contraction of pairs of anyonic operators. In the sequence of events marked (i), operator $\hat{A}$ is first raised to the space of three sites then contracted with $\hat{B}$. In sequence (ii) the operators are instead contracted using bends. For many anyon models the latter approach offers a significant computational advantage.

assignment of upward or downward direction is required. Second, all tensors must be represented by entirely convex shapes, such as circles or regular polygons. For existing tensor network algorithms such as MERA and PEPS, this requirement is trivial. However, it is conceivable that future algorithms might involve superoperator-type objects whose graphical representations interleave upward- and downward-pointing legs. Concavities on these objects may be eliminated by replacing some of their upward-pointing legs with downward-pointing legs (or vice versa), followed by a bend [Fig. 16, (i) and (ii)]. A similar treatment may be applied to any superoperators which arise during manipulations of the tensor network, introducing a pair of bends as in Fig. 12, (i) and then absorbing one into the matrix representation of the object.

If working with an anyon model that has nontrivial Frobenius-Schur indicators, then indicator flags must be applied to all bends. Initial choices are a matter of convenience, and it is frequently possible to assign these indicators in opposed pairs, as shown in Fig. 12. If these paired indicators are not flipped or are only flipped in adjacent opposed pairs during subsequent manipulations of the tensor network, then they may frequently be left implicit.

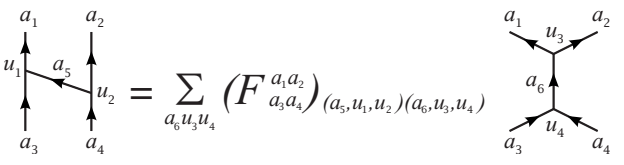

FIG. 15. Now that we may bend legs up and down it is customary to introduce a further type of F move, derived by applying bends to the one presented in Fig. 1, (iii).

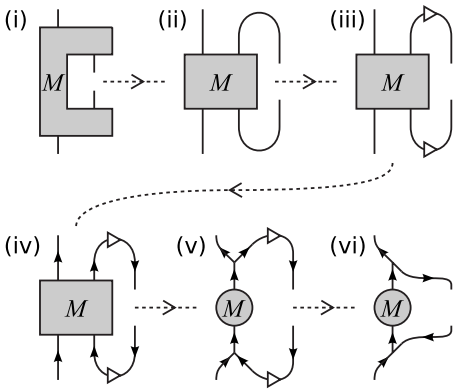

FIG. 16. Construction of an anyonic tensor corresponding to a normal tensor with more than three legs. (i) The original tensor. (ii) If required, any concavities are eliminated by introducing bends. (iii) Frobenius-Schur indicators are assigned to the bends. (iv) Directions are assigned to all legs, consistent with the rest of the network. (v) Legs are collected together into fusion and splitting trees. The central object, representing degrees of freedom of the tensor, now has less than four legs. (vi) If desired, bends can be reabsorbed into the fusion and splitting trees.

Next, if there exist charges in the anyon model which are not self-dual, a direction (represented by a solid arrow) must be assigned to every multi-index. Any tensor with more than three legs (e.g., M in Fig. 16) is then replaced by a trivalent tensor network consisting of a core object, e.g., M^{β}_{α}, which contains the free parameters of the tensor, and as many copies of $\tilde{N}$ or $\tilde{N}^{\dagger}$ as are required to provide the correct output legs. These tensors $\tilde{N}$ and $\tilde{N}^{\dagger}$ correspond to vertices in the fusion and splitting trees associated with M^{β}_{α}, yielding the corresponding anyonic tensor. Objects with three legs or less can be directly identified with an anyonic tensor object carrying the appropriate number of indices (i.e., three multi-indices and a vertex index u), though for consistency with the methods described in Secs. IV B and IV C we point out that it is possible to similarly replace three-legged objects with anyonic operators consisting of a central matrix M^{β}_{α} and a fusion or splitting vertex, if desired.

Any bends introduced earlier may now be reabsorbed so that some vertices now correspond to $(\tilde{N}^{\mathrm{CW}})$, $(\tilde{N}^{\mathrm{CCW}})$, $(\tilde{N}^{\mathrm{CW}})^{\dagger}$, and $(\tilde{N}^{\mathrm{CCW}})^{\dagger}$. This step, however, is optional as it may be more convenient for subsequent manipulations of the tensor network if the bends are left explicit. The anyonic tensors are then connected precisely as in the original ansatz.

Manipulations of the anyonic tensor network are equivalent to those performed on the spin version of the ansatz, differing only in that the degrees of freedom of the tensor network are now expressed entirely by the at-most-trivalent central objects, and certain topological elements such as braids and vertical bends must be accounted for in accordance with the prescriptions of Sec. IV C. These changes may naturally imply minor changes to the manipulation algorithms, and we will see examples of this in the 1D MERA. Similar considerations will apply to other tensor network algorithms.

Our construction of an anyonic tensor network draws upon two important elements which have previously been observed in other, simpler, physical systems:

(1) Tensors in the ansatz exhibit a global symmetry, which may be non-Abelian. Exploiting a non-Abelian symmetry requires that the ansatz be written in the form of a trivalent tensor network. This has previously been observed and implemented for non-Abelian Lie group symmetries such as $SU(2)$.[30]

(2) Tensors in the ansatz must be able to account for nontrivial exchange statistics. This has previously been observed in the simulation of systems of fermions,[31–38] where efficient implementation of particle statistics can be achieved through the use of "swap gates."[33–35,37]

In both cases, anyonic tensor networks extend the concepts introduced in previous work. The symmetry structure of an anyon model may be a quantum group, for example, a member of the series $SU(2)_k$, $k \in \mathbb{Z}^+$, rather than having to be a Lie group, and this permits representation of non-Abelian anyonic systems whose Hilbert space does not admit decomposition into a tensor product of local Hilbert spaces. Similarly, anyonic braiding may be implemented using a generalization of the fermionic swap gate formalism. When braiding, particle exchange may introduce transformation by a unitary matrix rather than by a sign, and efficient implementation of the resulting swap gates is particularly important for the simulation of 2D systems.

Although anyonic systems pose a number of unique challenges, we see that these are addressed by developments based on existing techniques, and we therefore anticipate that the resulting generalizations of existing tensor network ansätze should still be capable of accurately representing the states of an anyonic system.

E. Contraction of anyonic tensor networks

The techniques described in Secs. IV B and IV C (*F* moves, braids, bending of legs, elimination of loops, diagrammatic isotopy, flipping of Frobenius-Schur indicator flags, and the use of $\tilde{N}^{(\dagger)}$ tensors) suffice to contract any network of anyonic tensors written in the form of matrices with degeneracy indices, and unlabeled trees. Through careful application of these techniques, and avoiding at all times processes which would yield a tensor with more than three legs, the matrix representations of any pair of contiguous tensors in a network may always be brought into conjunction such that their multi-indices can be contracted in the manner of Eq. (12), and any tensor network may be contracted by means of a sequence of such pairwise contractions.

That a tensor network may represent a system of anyons in this way is possible because throughout the anyonic tensor network, each value of a degeneracy index is associated with a specific labeling of the corresponding unlabeled tree. Consequently it is always possible to fully reconstruct any operation in terms of the more verbose representation of Fig. 4.

An anyonic tensor network is therefore fully specified merely by the unlabeled tree (with Frobenius-Schur indicator flags if required), and the values and locations of the matrix representations of its tensors, written in the degeneracy index form.

V. EXAMPLE: THE 1D MERA

A. Construction

To construct an anyonic MERA for a 1D lattice with n sites, where n satisfies $n=2\times 3^k$, $k \in \mathbb{Z}^+$, we begin with a "top" tensor on a two-site lattice $\mathcal{L}_\tau$ whose matrix representation is of a computationally convenient size. (The top tensor is named for its position in the usual diagrammatic representation of the MERA, where diagrams with open legs at the bottom correspond to a ket. For anyons the converse convention applies, and consequently in Fig. 17, (i) the top tensor is ironically located at the bottom.)

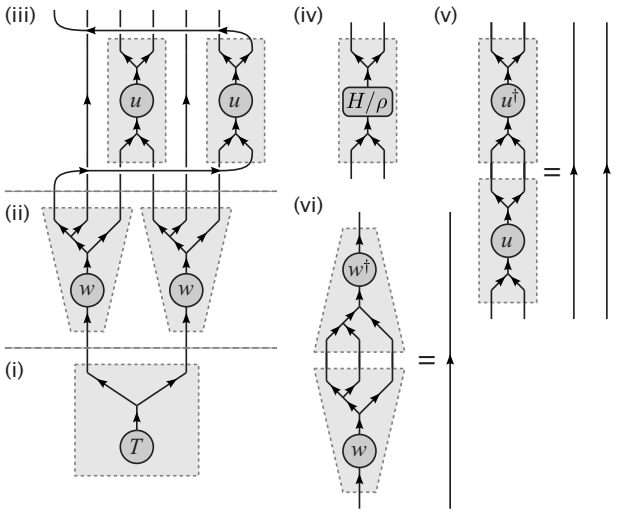

FIG. 17. Construction of a 1D ternary MERA on a periodic lattice from anyonic operators. (i) The top tensor, $\hat{T}$. (ii) Isometries, $\hat{w}$. (iii) Disentanglers, $\hat{u}$. The fusion tree representing an anyonic state (or ket) is usually drawn with the lattice sites at the top, so this MERA has been constructed "upside down" when compared with the diagrams in Refs. 23 and 27. This is unimportant, and we could equally well have decided to follow the convention usually adopted in tensor network algorithms, labeled the tensors in (i)–(iii) by $T^\dagger$, $w^\dagger$, and $u^\dagger$, and identified diagram (i)–(iii) as a bra. (iv) Structure of a two-site term in the Hamiltonian, $\hat{h}$, or a two-site reduced density matrix, $\hat{\rho}$. (v) Disentanglers and (vi) isometries satisfy the relationships $\hat{u}\hat{u}^\dagger=\mathbb{I}$ and $\hat{w}\hat{w}^\dagger=\mathbb{I}$.

To each leg of the top tensor, we now append an isometry [Fig. 17, (ii)]. The matrix representations of the isometries consist of rectangular blocks, as described in Sec. III B, and we choose isometries whose fusion trees have three legs, so as to construct a ternary MERA.[27] Next, disentanglers are applied above the isometries. For periodic boundary conditions this must be performed in a manner which respects the anyonic braiding rules, as shown in Fig. 17, (iii). We identify the open legs of the resulting network as the sites of a lattice $\mathcal{L}_{\tau-1}$, and the rows of disentanglers and isometries may be understood as a coarse-graining transformation taking a finer-grained lattice $\mathcal{L}_{\tau-1}$ into a coarser-grained lattice $\mathcal{L}_\tau$, similar to the standard MERA. Note that the geometry of the periodic lattice is reflected by the connections of the disentanglers. Specifically, whether the outside legs are braided over or under the other lattice sites reflect whether the lattice closes toward or away from the observer.

The application of anyonic isometries and disentanglers is now repeated k times [Fig. 17, (i)–(iii) corresponds to $k=1$], until the ansatz has n legs. The final row of isometries should be chosen such that each of their upper legs have the same charges and degeneracies as the sites of the physical lattice

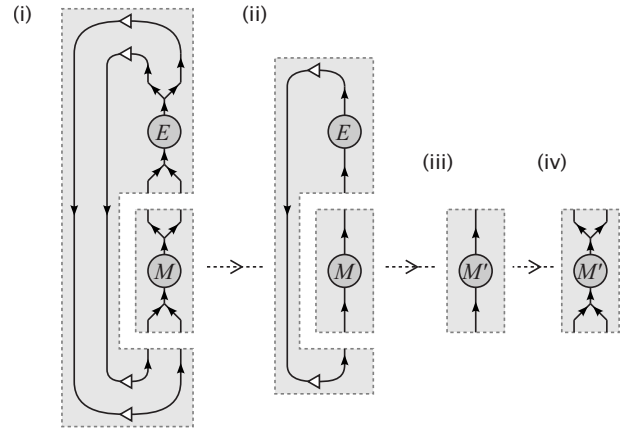

FIG. 18. (i) Anyonic operator $\hat{E}$ constitutes the environment of operator $\hat{M}$. Factors arising from the fusion and splitting trees should be evaluated and absorbed into matrices E and M, following which (ii) matrix E constitutes the environment of matrix M. After (iii) updating the matrix M to M', (iv) the fusion and splitting trees of $\hat{M}$ should be reinstated, the numerical factors associated with this process being the inverse of the fusion tree factors previously absorbed into matrix M. Frobenius-Schur flags in (i) and (ii) are represented by white triangles and are not to be confused with the black arrows which indicate the orientation of lines in the fusion/splitting trees.

$\mathcal{L}_0$, and the open legs above the last row of disentanglers are identified with the physical lattice. For coarse-grained lattices $\mathcal{L}_1$ to $\mathcal{L}_\tau$, the dimensions of the lattice sites correspond to the lower legs of the isometries and are chosen for computational convenience, subject to the requirement that each

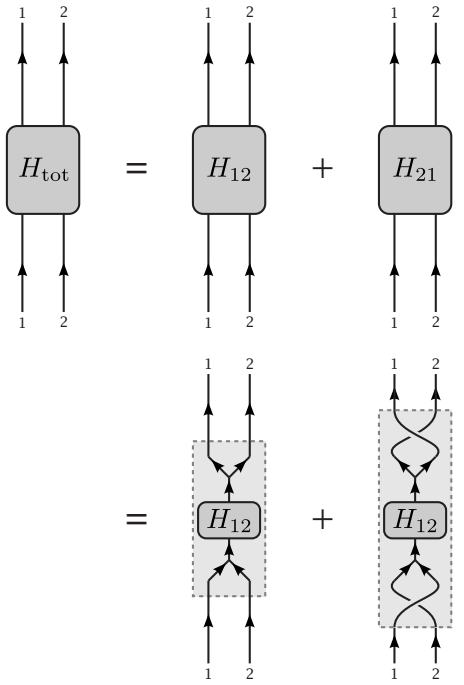

FIG. 19. Definition of $\hat{H}_{21}$ in terms of $\hat{H}_{12}$, on the most coarse-grained lattice ($\mathcal{L}_\tau$) of the translation-invariant periodic MERA. Lattice $\mathcal{L}_\tau$ is a two-site periodic lattice.

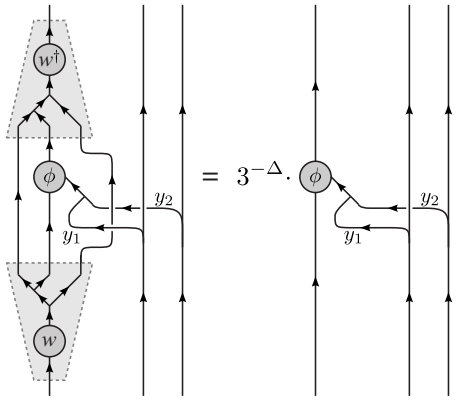

FIG. 20. Determination of eigenoperators (φ) and associated scaling dimensions (Δ) for the one-site scaling superoperator of the anyonic 1D MERA. Eigenoperators may be classified according to the charges on edges y_1 and y_2. One interpretation of these labels is that, in addition to the sites of the 1D lattice, there may exist free charges lying in front of and behind the anyon chain. The labels y_1 and y_2 then represent the transfer of charge between these regions and the 1D lattice.

charge sector is sufficiently large to adequately reproduce the physics of the low-energy portion of the Hilbert space. For all other legs, their charges and degeneracies are determined by requiring consistency with Eq. (2). Initial choices of which charges to represent on the top tensor and on the lower legs of the isometries, and with what degeneracies, must be guided either by prior knowledge about the physical system, or by balancing computational convenience against the inclusion of a broad and representative range of possible charges. When used in a numerical optimization algorithm, the choice of relative weightings for the different charge sectors may often be refined by examination of the spectra of the reduced density matrices on the coarse-grained lattices, after initial optimization of the tensor network is complete.

This concludes construction of the MERA for a state on a finite, periodic 1D anyonic lattice. That this tensor network does represent an anyonic state is easily seen by sequentially raising tensors, performing F moves, and combining tensors, until the entire network is reduced to a single vector whose length is equal to the dimension of the physical Hilbert space, and an associated fusion tree. These then represent the state of the system as per Eq. (4). The structure of this tensor network closely resembles that of the normal MERA, according to the identifications given in Fig. 17, and consequently we anticipate that it will share many of the same properties, including the ability to reproduce polynomially decaying correlators in strongly correlated physical systems. Open lattices may also be easily represented by omitting the braided disentanglers at the edge of the diagram.

We also note that in common with the MERA for spins, the anyonic MERA may be understood as a quantum circuit, although one which carries anyonic charges in its wires. Any junction in the fusion/splitting trees may be associated with a $\tilde{N}$ or $\tilde{N}^\dagger$ tensor, and the entire network may be considered as the application of a series of gates to a Hilbert space of fixed dimension beginning mostly (or entirely, if the top tensor is considered to be the first gate) in the vacuum state, with

TABLE III. Scaling dimensions for Fibonacci anyons with antiferromagnetic nearest-neighbor interactions on an infinite chain. Numerical values were computed using an anyonic MERA with maximum degeneracies for charges 1 and τ of 3 and 5, respectively (denoted $\chi=[3,5]$), and are grouped according to their classification by the values of y_1 and y_2 in Fig. 20.

Exact	Numerics	Error (%)
	$y_1=y_2=1$	
0	0	0
7/8	0.8995	+2.80
7/8+1	1.9096	+1.85
7/8+1	1.9141	+2.09
0+2	2.0124	+0.62
0+2	2.0181	+0.90
	$y_1=y_2=\tau$	
3/40	0.0751	+0.19
1/5	0.2006	+0.28
3/40+1	1.0730	−0.19
3/40+1	1.0884	+1.25
6/5	1.2026	+0.21
1/5+1	1.2156	+1.30
	$y_1=1$, $y_2=\tau$	
19/40	0.4757	+0.14
3/5	0.6009	+0.15
19/40+1	1.4549	−1.37
19/40+1	1.5022	+1.85
3/5+1	1.5414	−3.66
3/5+1	1.6129	+0.80
	$y_1=\tau$, $y_2=1$	
19/40	0.4757	+0.14
3/5	0.6009	+0.15
19/40+1	1.4549	−1.37
19/40+1	1.5022	+1.85
3/5+1	1.5414	−3.66
3/5+1	1.6129	+0.80

TABLE IV. Scaling dimensions for Fibonacci anyons with ferromagnetic nearest-neighbor interactions on an infinite chain. Numerical values were computed using an anyonic MERA with maximum degeneracies for charges 1 and τ of 3 and 5, respectively (denoted $\chi=[3,5]$), and are grouped according to their classification by the values of y_1 and y_2 in Fig. 20.

Exact	Numerics	Error (%)
	$y_1=y_2=1$	
0	0	0
4/3	1.3514	+1.36
4/3	1.3695	+2.71
0+2	1.9519	−2.41
0+2	1.9742	−1.29
1+4/3	2.2570	−3.27
	$y_1=y_2=\tau$	
2/15	0.1329	−0.35
2/15	0.1339	+0.44
4/5	0.8134	+1.67
2/15+1	1.0937	−3.49
2/15+1	1.1108	−1.99
2/15+1	1.1622	+2.55
	$y_1=1$, $y_2=\tau$	
2/5	0.3993	−0.18
11/15	0.7327	−0.09
11/15	0.7392	+0.80
2/5+1	1.3699	−2.15
2/5+1	1.3823	−1.26
11/15+1	1.6450	−5.10
	$y_1=\tau$, $y_2=1$	
2/5	0.3993	−0.18
11/15	0.7327	−0.09
11/15	0.7392	+0.80
2/5+1	1.3699	−2.15
2/5+1	1.3823	−1.26
11/15+1	1.6450	−5.10

individual gates introducing entanglement across some limited number of wires.

B. Energy minimization

The anyonic MERA can be used as a variational ansatz to compute the ground state of a local Hamiltonian. The Hamiltonian is introduced as a sum over nearest-neighbor interactions, each term having the form of Fig. 17, (iv), and optimization of the tensor network is carried out in the usual manner.[27] Also as per usual, Hamiltonians involving larger interactions, such as next-to-nearest neighbor, can be accommodated by means of an initial exact n-into-one coarse graining of the physical lattice.

As in Ref. 27, optimization of the MERA then consists of repeatedly lifting the Hamiltonian from $\mathcal{L}_0$ to the coarse-grained lattices, updating their isometries and disentanglers, and lowering the reduced density matrix, or the top tensor and its conjugate. When lifting the Hamiltonian or lowering the reduced density matrix, then the diagrams in Ref. 27 taken in conjunction with the key given in Fig. 17 serve to describe networks of anyonic operators which, when contracted to a single operator, yield the lifted form of the Hamiltonian or lowered form of the reduced density matrix, respectively. Similarly, when optimizing disentanglers or isometries, the diagrams of Ref. 27 and the identifications in Fig. 17 indicate how to construct an anyonic operator which constitutes the environment of the anyonic operator being

optimized. However, once the admissible ranges of charges and degeneracies on each leg have been fixed, the only optimizable content of an anyonic operator is its matrix representation. Consequently, the fusion and splitting tree contributions should be evaluated and absorbed into the operator and its environment, reducing them both to their matrix representations, denoted M and E, respectively (see Fig. 18). If the singular value decomposition of E is written $E=USW^\dagger$, then the updated matrix content M of the anyonic operator being optimized is given by $-WU^\dagger$, minimizing the value of $\mathrm{Tr}(EM)$ subject to the usual constraint for disentanglers and isometries that $\hat{M}\hat{M}^\dagger=\mathbb{I}$ [Fig. 17, (v) and (vi)]. The fusion/splitting tree content of the operator can then be restored, along with any appropriate numerical factors that may be required.

As with the standard MERA, the top tensor is constructed by diagonalizing the total Hamiltonian on the most coarse-grained lattice, $\hat{H}_{\mathrm{tot}}$ on $\mathcal{L}_\tau$. As $\mathcal{L}_\tau$ is a two-site lattice, the total Hamiltonian $\hat{H}_{\mathrm{tot}}$ is a sum of two terms, $\hat{H}_{12}$ and $\hat{H}_{21}$. For the translation-invariant anyonic MERA, we may formally define $\hat{H}_{21}$ in terms of $\hat{H}_{12}$ as shown in Fig. 19, and the top tensor $\hat{T}$ (together with any factors arising from the chosen normalization scheme) then corresponds to the lowest-energy eigenstate of $\hat{H}_{\mathrm{tot}}$.

C. Scale invariant MERA

Having identified the anyonic counterparts of the tensors of the standard MERA, and described how these tensors may be lifted, lowered, and optimized, the algorithm for the scale-invariant MERA described in Ref. 26 may also be implemented for anyonic systems, simply by applying the dictionary of Fig. 17 and the techniques described in Sec. V B. As with optimization of $\hat{u}$ and $\hat{w}$, the computation of the top reduced density matrix (which is a descending eigenoperator of the scaling superoperator with eigenvalue 1) may be understood as a calculation of the matrix component ρ_α^β of the reduced density matrix $\hat{\rho}$. The ascending eigenoperators of the scaling superoperator, or local scaling operators of the theory, may also be computed in this manner.

D. Results

To demonstrate the effectiveness of the anyonic generalization of the MERA, we applied it to a 1D critical system of anyons whose physical properties are already well known: the golden chain.[4] This model consists of a string of Fibonacci anyons subject to a local interaction. Fibonacci anyons have only two charges, 1 (the vacuum) and τ, and one nontrivial fusion rule ($\tau\times\tau\to 1+\tau$). The simplest local interactions for a chain of Fibonacci τ anyons are nearest-neighbor interactions favoring fusion of pairs into either the 1 channel (termed antiferromagnetic, or AFM), or the τ channel (termed ferromagnetic, or FM). Both choices correspond to critical Hamiltonians, associated with the conformal field theories $\mathcal{M}(4,3)$ and $\mathcal{M}(5,4)$ for AFM and FM couplings, respectively. Individual lattice sites are each associated with a charge of τ.

The AFM and FM Hamiltonians act on pairs of adjacent Fibonacci anyons. On a pair of lattice sites each carrying a charge of τ, the matrix representations of the AFM and FM Hamiltonians are written

$$(H_\alpha^\beta)_{\mathrm{AFM}}=\begin{pmatrix}-1 & 0\\ 0 & 0\end{pmatrix}\quad (H_\alpha^\beta)_{\mathrm{FM}}=\begin{pmatrix}0 & 0\\ 0 & -1\end{pmatrix}, \tag{17}$$

where a multi-index value of 1 corresponds to the vacuum charge, 2 corresponds to τ, and the charges are nondegenerate. We optimized a scale-invariant MERA on the golden chain for each of these Hamiltonians, and computed local scaling operators using the tensor network given in Fig. 20. The operators calculated using this diagram may be classified according to the values of the charge labels y_1 and y_2, and the scaling dimensions and conformal spins which we

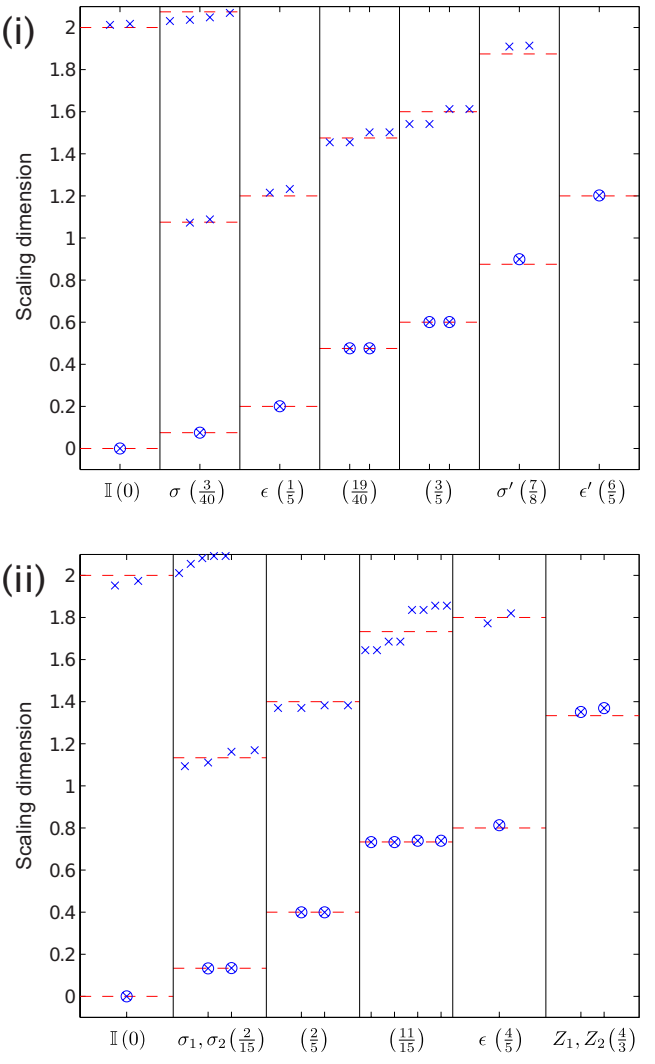

FIG. 21. (Color online) Scaling dimensions of leading primary operators and their descendants, computed for (i) antiferromagnetic and (ii) ferromagnetic local Hamiltonians (17) on the golden chain. Results are grouped into conformal towers, with a slight horizontal spread introduced to show the degeneracies of the descendant fields. A circled cross indicates a primary field, and a plain cross indicates a descendant. Dashed lines indicate values predicted from CFT.

obtained are given in Tables III and IV, and Fig. 21.

Comparison of the AFM case with existing results in the literature show that the scaling dimensions obtained when $y_1=y_2$ correspond to those obtained when studying a system of anyons with a toroidal fusion diagram.[4] For a system of anyons on the torus it is possible to define an additional topological symmetry[4] and classify local scaling operators according to whether or not they respect this symmetry. Operators satisfying $y_1=y_2=1$ correspond to those which respect the topological symmetry, and those satisfying $y_1=y_2=\tau$ do not. We will discuss the interpretation of the different sectors and their relationship to anyons on the torus in a forthcoming paper.[39] When $y_1\neq y_2$ the scaling operators obtained are chiral, with those obtained from $y_1=1$, $y_2=\tau$ and $y_1=\tau$, $y_2=1$ believed to form conjugate pairs.

VI. SUMMARY

Numerical study of systems of interacting anyons is difficult due to their nontrivial exchange statistics. To date, study of these systems has been restricted to exact diagonalization, matrix product states for 1D systems, or special-case mappings to equivalent spin chains. This paper shows how any tensor network ansatz may be translated into a form applicable to systems of anyons, opening the door for the study of large systems of interacting anyons in both one and two dimensions. As an example, this paper demonstrates how the MERA may be implemented for a 1D anyonic system. This ansatz is particularly important as many 1D systems of anyons are known which exhibit extended critical phases.[4,8,40] The structure of the MERA is known to be particularly well suited to reproducing long-range correlations, and the scale-invariant MERA has the additional advantage of providing simple and direct means of computing the scaling dimensions and matrix representations of local scaling operators.

We applied the scale-invariant MERA to infinite chains of Fibonacci anyons under antiferromagnetic and ferromagnetic nearest-neighbor couplings, and identified a large number of local scaling operators. Our results for the scaling dimensions are in agreement with those previously obtained by exact diagonalization of closely related systems, and for the relevant primary fields they are within 2.8% of the theoretical values obtained from conformal field theory. We thus demonstrate that an anyonic MERA with $\chi=[3,5]$ permits conclusive identification of the relevant conformal field theory, and gives a level of accuracy comparable to that of the scale-invariant MERA on a spin chain.[26]

The anyonic generalization of the 1D MERA presented here is useful in its own right but the greatest significance of the approach described is that it is equally applicable to 2D tensor network ansätze, and hence opens the door to studying the collective behavior of large systems of anyons in two dimensions by numerical means, in situations where analytical solutions may not be possible.

Note added. While preparing this paper for publication, we became aware of related work by König and Bilgin.[41] They also present the anyonic 1D MERA, providing proof of principle by computing ground-state energies for finite systems of Fibonacci anyons with $\chi=[1,1]$ ($s=2$ in their notation).

ACKNOWLEDGMENTS

The authors acknowledge the support of the Australian Research Council (Grants No. FF0668731, No. DP0878830, and No. DP1092513, APA). This research was supported in part by the Perimeter Institute for Theoretical Physics.

*pfeifer@physics.uq.edu.au

[1] A. Y. Kitaev, Ann. Phys. **303**, 2 (2003).
[2] C. Nayak, S. H. Simon, A. Stern, M. Freedman, and S. Das Sarma, Rev. Mod. Phys. **80**, 1083 (2008).
[3] J. S. Xia, W. Pan, C. L. Vicente, E. D. Adams, N. S. Sullivan, H. L. Stormer, D. C. Tsui, L. N. Pfeiffer, K. W. Baldwin, and K. W. West, Phys. Rev. Lett. **93**, 176809 (2004).
[4] A. Feiguin, S. Trebst, A. W. W. Ludwig, M. Troyer, A. Kitaev, Z. Wang, and M. H. Freedman, Phys. Rev. Lett. **98**, 160409 (2007).
[5] S. R. White, Phys. Rev. Lett. **69**, 2863 (1992).
[6] G. Sierra and T. Nishino, Nucl. Phys. B **495**, 505 (1997).
[7] W. Tatsuaki, Phys. Rev. E **61**, 3199 (2000).
[8] S. Trebst, E. Ardonne, A. Feiguin, D. A. Huse, A. W. W. Ludwig, and M. Troyer, Phys. Rev. Lett. **101**, 050401 (2008).
[9] F. C. Alcaraz, M. N. Barber, M. T. Batchelor, R. J. Baxter, and G. R. W. Quispel, J. Phys. A **20**, 6397 (1987).
[10] S. Todo and K. Kato, Phys. Rev. Lett. **87**, 047203 (2001).
[11] F. Verstraete and J. I. Cirac, arXiv:cond-mat/0407066 (unpublished).
[12] T. Nishino and K. Okunishi, J. Phys. Soc. Jpn. **67**, 3066 (1998).
[13] Z.-C. Gu, M. Levin, and X.-G. Wen, Phys. Rev. B **78**, 205116 (2008).
[14] H. C. Jiang, Z. Y. Weng, and T. Xiang, Phys. Rev. Lett. **101**, 090603 (2008).
[15] J. Jordan, R. Orús, G. Vidal, F. Verstraete, and J. I. Cirac, Phys. Rev. Lett. **101**, 250602 (2008).
[16] L. Tagliacozzo, G. Evenbly, and G. Vidal, Phys. Rev. B **80**, 235127 (2009).
[17] L. Cincio, J. Dziarmaga, and M. M. Rams, Phys. Rev. Lett. **100**, 240603 (2008).
[18] G. Evenbly and G. Vidal, Phys. Rev. Lett. **102**, 180406 (2009).
[19] G. Evenbly and G. Vidal, Phys. Rev. Lett. **104**, 187203 (2010).
[20] P. Di Francesco, P. Mathieu, and D. Sénéchal, *Conformal Field Theory* (Springer, New York, 1997).
[21] G. Vidal, Phys. Rev. Lett. **99**, 220405 (2007).
[22] G. Vidal, Phys. Rev. Lett. **101**, 110501 (2008).
[23] G. Vidal, in *Understanding Quantum Phase Transitions*, edited by L. D. Carr (Taylor & Francis, Boca Raton, 2010).
[24] X. Chen, Z. Gu, and X. Wen, arXiv:1004.3835 (unpublished).
[25] V. Giovannetti, S. Montangero, and R. Fazio, Phys. Rev. Lett. **101**, 180503 (2008).

[26] R. N. C. Pfeifer, G. Evenbly, and G. Vidal, Phys. Rev. A **79**, 040301 (2009).
[27] G. Evenbly and G. Vidal, Phys. Rev. B **79**, 144108 (2009).
[28] A. Kitaev, Ann. Phys. **321**, 2 (2006).
[29] P. H. Bonderson, Ph.D. thesis, California Institute of Technology, 2007.
[30] S. Singh, R. N. C. Pfeifer, and G. Vidal, arXiv:0907.2994 (unpublished).
[31] P. Corboz, G. Evenbly, F. Verstraete, and G. Vidal, Phys. Rev. A **81**, 010303 (2010).
[32] C. V. Kraus, N. Schuch, F. Verstraete, and J. I. Cirac, Phys. Rev. A **81**, 052338 (2010).
[33] C. Pineda, T. Barthel, and J. Eisert, Phys. Rev. A **81**, 050303(R) (2010).
[34] P. Corboz, R. Orus, B. Bauer, and G. Vidal, Phys. Rev. B **81**, 165104 (2010).
[35] T. Barthel, C. Pineda, and J. Eisert, Phys. Rev. A **80**, 042333 (2009).
[36] Q. Shi, S. Li, J. Zhao, and H. Zhou, arXiv:0907.5520 (unpublished).
[37] I. Pižorn and F. Verstraete, Phys. Rev. B **81**, 245110 (2010).
[38] Z. Gu, F. Verstraete, and X. Wen, arXiv:1004.2563 (unpublished).
[39] R. N. C. Pfeifer *et al.* (unpublished).
[40] S. Trebst, M. Troyer, Z. Wang, and A. W. W. Ludwig, Prog. Theor. Phys. Suppl. **176**, 384 (2008).
[41] R. König and E. Bilgin, arXiv:1006.2478 (unpublished).